CrossMark

A theoretical model of strong and moderate El Niño regimes

Ken Takahashi[1] · Christina Karamperidou[2] · Boris Dewitte[3,4,5]

Abstract

The existence of two regimes for El Niño (EN) events, moderate and strong, has been previously shown in the GFDL CM2.1 climate model and also suggested in observations. The two regimes have been proposed to originate from the nonlinearity in the Bjerknes feedback, associated with a threshold in sea surface temperature (T_c) that needs to be exceeded for deep atmospheric convection to occur in the eastern Pacific. However, although the recent 2015–16 EN event provides a new data point consistent with the sparse strong EN regime, it is not enough to statistically reject the null hypothesis of a unimodal distribution based on observations alone. Nevertheless, we consider the possibility suggestive enough to explore it with a simple theoretical model based on the nonlinear Bjerknes feedback. In this study, we implemented this nonlinear mechanism in the recharge-discharge (RD) ENSO model and show that it is sufficient to produce the two EN regimes, i.e. a bimodal distribution in peak surface temperature (T) during EN events. The only modification introduced to the original RD model is that the net damping is suppressed when T exceeds T_c, resulting in a weak nonlinearity in the system. Due to the damping, the model is globally stable and it requires stochastic forcing to maintain the variability. The sustained low-frequency component of the stochastic forcing plays a key role for the onset of strong EN events (i.e. for $T > T_c$), at least as important as the precursor positive heat content anomaly (h). High-frequency forcing helps some EN events to exceed T_c, increasing the number of strong events, but the rectification effect is small and the overall number of EN events is little affected by this forcing. Using the Fokker–Planck equation, we show how the bimodal probability distribution of EN events arises from the nonlinear Bjerknes feedback and also propose that the increase in the net feedback with increasing T is a necessary condition for bimodality in the RD model. We also show that the damping strength determines both the adjustment time-scale and equilibrium value of the ensemble spread associated with the stochastic forcing.

Keywords El Niño · ENSO · Nonlinearity · Bjerknes feedback · Recharge-discharge model · Fokker–Planck equation · Eastern Pacific

✉ Ken Takahashi
  ken.takahashi.guevara@gmail.com

Extended author information available on the last page of the article

1 Introduction

Theoretical models can be powerful tools to demonstrate the essential characteristics of a phenomenon, and can provide conceptual frameworks that guide further research, even if they are not capable of simulating every aspect of the dynamics of said phenomenon. In the case of El Niño-Southern Oscillation (ENSO), the main two conceptual models are the delayed oscillator (Suarez and Schopf 1988; Battisti and Hirst 1989) and the recharge-discharge oscillator (Jin 1997). These models provide simple mathematical representations of how slow ocean dynamics interact with the fast tropical atmosphere to produce ENSO variability, at least as measured in the simplest way with a single equatorial Pacific sea surface temperature (SST) anomaly index.

More recently, there has been a focus on the diversity among ENSO events (e.g. Capotondi et al. 2015), with most efforts focused on classifying EN events according to their spatial SST anomaly pattern, particularly whether they peak in the eastern or central Pacific (e.g. Larkin and Harrison 2005; Ashok et al. 2007; Kug et al. 2009; Takahashi et al. 2011). Alternatively or complementarily, ENSO events can be classified in terms of their intensity, e.g. strong vs moderate (Takahashi et al. 2011; Capotondi et al. 2015; Takahashi and Dewitte 2016, hereafter TD16). Here we focus on the latter, particularly on our proposal that strong EN events (e.g. 1982–83 and 1997–98) correspond to a separate dynamical regime associated with nonlinearity in the Bjerknes feedback (TD16). We found in observations and the GFDL CM2.1 climate model that the convection and the zonal wind stress response to the surface warming in the eastern equatorial Pacific is a factor of three larger when the SST anomaly exceeds a positive (non-zero) threshold that corresponds to an absolute SST of around 27.5 °C, consistent with previous studies on the activation of convection (Graham and Barnett 1987). In the eastern Pacific, this threshold marks the transition from the typically stable regime over the equatorial cold tongue to the deep convective regime mainly associated with the extreme El Niño events. In the CM2.1, EN events were shown to have a bimodal distribution, with the local antimode that separates the two modes corresponding to a eastern Pacific SST anomaly consistent with the threshold SST found for the nonlinear Bjerknes feedback enhancement. It should be noted, however, that the recent 2015–16 EN event showed that extreme warming in the far-eastern Pacific is not a necessary condition for EN to become strong (L'Heureux et al. 2016; Dewitte and Takahashi 2017). Thus, in order to build a theoretical model of the two EN regimes, to first approximation it may not be necessary to explicitly consider the spatial distribution of the anomalies.

Although empirical high-dimensional linear ENSO models can reproduce the diversity in the SST patterns by random processes alone (Newman et al. 2011), they can only simulate the asymmetry between of strong EN and La Niña (LN) events if nonlinearities are introduced (Chen et al. 2016). The nonlinearity in the Bjerknes feedback has already been invoked in previous studies to explain the asymmetry in magnitude and duration between El Niño and La Niña (Frauen and Dommenget 2010; Dommenget et al. 2012; Choi et al. 2013, 2015). A theoretical model with nonlinear ocean advection (Timmermann et al. 2003; An and Jin 2004) produces strong EN in the form of "bursts" as part of complex self-sustained nonlinear oscillations, but these only have a weak resemblance to observations. Furthermore, the nonlinear advection appears more relevant for the maintenance rather than for the growth of EN in nature (Su et al. 2010; TD16). It has also been been suggested that tropical instability waves provide a weaker damping El Niño (An

2008) and that ocean waves could respond stronger to the winds also during El Niño (An and Kim 2017). Another nonlinearity that can amplify warm EN events is "multiplicative forcing", by which the amplitude of the stochastic forcing is enhanced as T increases, either only the positive (westerly wind burst) forcing (Roulston and Neelin 2000; Eisenman et al. 2005; Gebbie et al. 2007; Gebbie and Tziperman 2009) or both positive and negative phases of the forcing (Levine and Jin 2010, 2015; Levine et al. 2016). Although all these nonlinear mechanisms could contribute to ENSO, no study to our knowledge has addressed the origin of strong and moderate dynamical regimes of El Niño (warm) events. For this, we introduce T_c greater than zero, which from a dynamical perspective is an important qualitative difference from previous studies because it introduces an asymmetry within El Niño itself rather than between El Niño and La Niña.

In this paper, we build upon the simplest version of the recharge-discharge (RD) ENSO model (Jin 1997; Burgers et al. 2005) in order to create a minimal ENSO model that can simulate strong and moderate EN regimes. We do so by suppressing the net damping that results from the Bjerknes and other feedbacks acting on T whenever the latter exceeds a positive threshold T_c, which can be qualitatively interpreted as the value required for the eastern Pacific absolute SST to exceed 27.5 °C (TD16). This model focuses only on the strength of El Niño events as a first approximation to ENSO diversity, neglecting the spatial distribution or seasonal effects, or nonlinear processes specific to La Niña. We consider state-independent (additive) forcing, although we briefly address the effect of multiplicative forcing. Despite the strong simplifications, we show that this model reproduces two EN regimes and provides insights into the role of the stochastic forcing in El Niño diversity and predictability.

2 Recharge-discharge model

Our stochastically-forced nonlinear RD oscillator is given by:

$$\frac{d}{dt}\begin{pmatrix} T \\ h \end{pmatrix} = \begin{pmatrix} a_{NL} & b \\ c & 0 \end{pmatrix}\begin{pmatrix} T \\ h \end{pmatrix} + F_0\begin{pmatrix} \varepsilon(t) \\ \zeta(t) \end{pmatrix}, \qquad (1)$$

where T is interpreted as the SST anomaly (K) in the Niño 3 region (150°W–90°W, 5°S–5°N) and h is the mean equatorial 20 °C isotherm depth anomaly (in decameters or dam; 140°E–80°W, 5°S–5°N), approximately equivalent to the mean thermocline depth or heat content anomaly. This is almost identical to the "simplest" recharge-discharge model of Burgers et al. (2005) except that the coefficient of T in the T-budget is nonlinear:

$$a_{NL} = \begin{cases} a, & T \leq T_c \\ 0, & T > T_c, \end{cases} \qquad (2)$$

i.e. the damping is deactivated when T exceeds T_c.

Since the mean climatological Niño 3 SST is 26 °C, if we take T_c as the value needed to reach 27.5 °C in order to activate the enhanced Bjerknes feedback (TD16) then $T_c = 1.5$ K. In addition to the results discussed in the previous section, the analysis of recent (1995–2016) observed Niño 3 SST anomalies and eastern-central Pacific zonal wind pseudo-stress confirms the nonlinear relation with a threshold of around 1.3 K, consistent with our selection for T_c (Fig. 1). We also note that the 2015–2016 El Niño also shows the nonlinear enhancement even though the warming in the far-eastern Pacific was not as strong as in 1997–1998 (L'Heureux et al. 2016).

We note that a_{NL} is the net feedback, which not only includes the atmospheric component of the Bjerknes feedback but also the adjusement of the thermocline and ocean currents, the damping by surface heat fluxes and cloud response (cf. the BJ index of Jin et al. 2006). This also includes the nonlinear radiative cloud feedback that enhances damping in the convective regime (Lloyd et al. 2012a; Bellenger et al. 2014). The empirical or physically-based estimation of the a_{NL} is a substantial problem in itself, which we have not attempted to address in this study. Instead we conservatively assume a neutral value
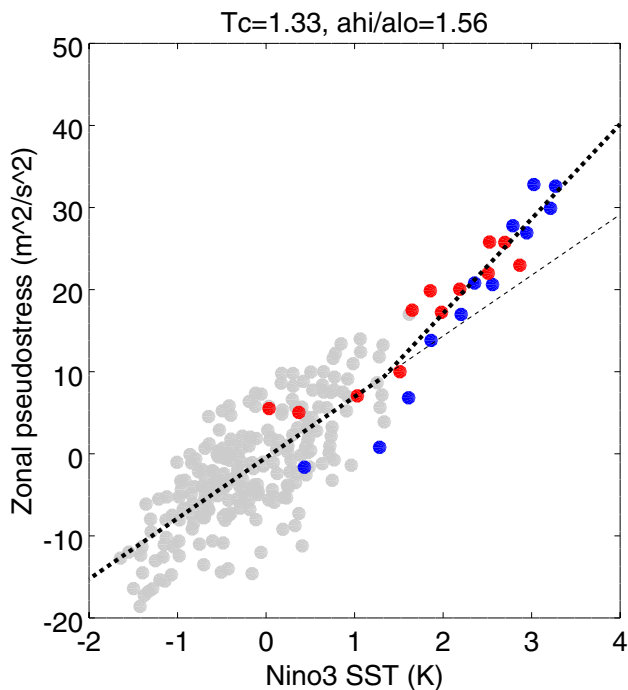

Fig. 1 Equatorial Pacific (180°–140°W, 5°S–5°N) pseudostress (estimated from monthly TAO wind speed and zonal wind data; McPhaden et al. 1998) and Niño 3 SST anomalies (ERSST v3b; Smith et al. 2008). The piecewise linear regression fit using ARE-SLab (Jekabsons 2013; following TD16) yields a threshold SST of T_c =1.33 K and a nonlinear enhancement of 56%. Blue and red dots correspond to July–June of 1997–1998 and 2015–2016, respectively

for $T > T_c$, although we do not rule out the possibility for positive growth rate in this regime. The stochastic forcing variability terms (ε and ζ) are given by monthly gaussian white-noise series, and are state-independent.

For simplicity, we set $\varepsilon = \zeta$ with unit variance so that the same forcing acts on T and h, based on the idea that the zonal wind forcing that drives the thermocline tilt that is tightly linked with T also produces h anomalies with the same sign. These anomalies are associated with the short-term Kelvin wave response, at least at intraseasonal time-scales, although the h response is sensitive to the time-scale and geographical pattern of the forcing (McGregor et al. 2015). The implementation of such details in the RD model is not straightforward and will be explored in future work.

All other parameters equal the empirical fits proposed by Burgers et al. (2005): $a = -0.076$ month^{-1}, $b = 0.236$ K dam^{-1} month^{-1}, $c = -0.125$ dam K^{-1} month^{-1}. Thus, for $T < T_c$, the model is the same damped oscillator of Burgers et al. (2005), while for $T > T_c$ it is a neutral recharge-discharge oscillator. Fitting the linear RD model to the nonlinear RD model run produces a weaker effective linear damping parameter to the original from Burgers et al. (2005), as expected. This reduced by 45% weaker damping that the Burgers et al. (2005). We use a value of $F_0 = 0.17$ K/month (or dam/month), which produces a standard deviation of T of 0.85 K, close to the observed for Niño 3 (0.90 K).

With these parameters, the decay time is 26.3 months for $T < T_c$ and neutral for $T > T_c$. The intrinsic oscillation periods are 35.7 for $T < T_c$ and 36.6 months for $T > T_c$. For $T < T_c$, this implies that in the deterministic case, the amplitude of oscillation would be reduced by 74% after each cycle, so stochastic forcing is essential to keep an oscillatory-like behavior in this regime. For states with $T > T_c$, the system is undamped, but the RD dynamics will eventually bring any state back to the damped regime, so the system is absolutely stable and requires stochastic forcing to maintain the variability. We also note that this model does not allow for multiple equilibria, as $T = h = 0$ is the only fixed point.

The model is solved numerically for 2×10^6 years using a fourth-order Runge-Kutta scheme and a full timestep of 1 month. The forcing series $\varepsilon(t)$ is a single realization of noise that is applied identically for all experiments, so that specific moments in time (particularly EN events) can be compared among experiments. The peak T for EN events were determined as the maximum value of the 1–2–1 filtered monthly T within running 2-year windows. Hereafter, the term strong EN refers to events with peak $T \geq 1.5$ K, while events with peak $0.5 < T < 1.5$ K are termed moderate.

The following experiments were performed: The control run (CTL) is as specified above. The linear (LIN) model run is the same as CTL except that the enhanced Bjerknes feedback is not active, so that $a_{NL} = a$ for all T. A low-passed forcing (LFF) experiment was done exactly as

CTL except that the time-series of ε was previously low-passed filtered with a cutoff period of 12 months using an 8th order Butterworth filter. A complementary experiment (indepF) has independent stochastic forcing series for T and h ($\varepsilon(t) \neq \zeta(t)$), while another one (FonlyT) has the forcing applied only to T (i.e. $\zeta(t) = 0$) scaled by a factor of 2. Additionally, to test whether multiplicative forcing (i.e. increasing forcing strength with T) can generate a bimodal EN distribution, we made experiments MULTLIN and MULT, which are equivalent to the LIN and CTL runs, respectively, except that we multiplied the forcing by $[1 + BH(T - T_c)(T - T_c)]$ where $B = 0.5$, and H is the Heaviside function ($H(x) = 0$ for $x < 0$ and $H(x) = 1$ for $x \geq 0$). This is based on Levine and Jin (2017) but, since this nonlinearity also originates from the threshold for deep convection, we set the state-dependence for $T > T_c$ instead of $T > 0$. Since the system becomes unstable, we limited $|T|$ to be < 7 K in the numerical solutions (equivalent to extremely strong nonlinear damping).

3 Fokker–Planck equation

The Fokker–Planck (FP) equation describes the evolution of the probability distribution function (PDF) of states in a sto-chastically-forced ("Brownian") dynamical system (Risken 1996), which allows us to address issues of predictability in simple climate models by describing how the PDF evolves from an initial condition under all possible realizations of the stochastic forcing (e.g. Hasselmann 1976). The system does not require the presence of deterministic divergence in phase-space, as measured with Lyapunov exponents (e.g. Karamperidou et al. 2013), in order for the ensemble to spread, as is the case with chaotic systems like the Lorenz system (e.g. Palmer 1993). Using the terminology of the FP equation, the PDF evolution is governed by the "drift", which is the displacement, rotation, and deformation of the PDF by the deterministic dynamics, and the "diffusion", which is the spreading of the PDF due to the random walk associated with the stochastic forcing.

Let ρ be the joint $T - h$ PDF for an ensemble of states that obey Eq. (1). The FP equation that describes its evolution in our non-linear RD model with the same forcing in T and h (i.e. forced along $\phi \equiv (T + h)/\sqrt{2}$ with amplitude $\sqrt{2}F_0$) is:

$$
\begin{aligned}
\frac{\partial \rho}{\partial t} =& -\frac{\partial[(a_{\mathrm{NL}}T + bh)\rho]}{\partial T} - \frac{\partial[(cT)\rho]}{\partial h} + F_0^2 \frac{\partial^2 \rho}{\partial \phi^2} \\
=& -a_{\mathrm{NL}}\rho - \frac{da_{\mathrm{NL}}}{dT}T\rho - (a_{\mathrm{NL}}T + bh)\frac{\partial \rho}{\partial T} - (cT)\frac{\partial \rho}{\partial h} + F_0^2 \frac{\partial^2 \rho}{\partial \phi^2}
\end{aligned}
$$
(3)

This is a conservation equation for ρ in an eulerian frame, with the first two terms on the right-hand side (rhs) in the first line describing the convergence of the transport of ρ by the deterministic dynamics, i.e. the drift. The third term

($F_0^2 \partial^2 \rho / \partial \phi^2$) is the stochastic diffusion term. In the second line, the drift term has been expanded to isolate different processes. The first term is the "damping term" that leads to the *growth* of ρ due to the convergence of the drift due to dissipation, by focusing the PDF into smaller areas in phase-space. We call the second term the "regime-shift term", which in our non-linear model is formulated with da_{NL}/dt idealized as a delta function at $T = T_c$ as a_{NL} goes from a to 0. The third and fourth terms correspond to advection and produce the displacement and rotation of the PDF.

We solved the FP equation numerically with a grid size of 0.05 in T and h and a time-step of 5×10^{-3} months for the domain $T \in [-6, 9]$ and $h \in [-6, 6]$ with no-flux boundary conditions. We used centered differences and fourth-order Runge-Kutta time-stepping, with 1–6–1 filtering in both T and h every 0.5 months to prevent the growth of the computational mode.

4 Results

4.1 El Niño bimodality

The peak T values for most of the EN are clustered below 1.5 K, but the peaks of the three strongest events (1982–1983, 1997–1998, 2015–2016) are clustered between 2.7 and 3.2 K (Fig. 2a). Only the 1972–1973 event is found in the large gap between them. As a result, the probability density function (PDF) estimated using kernels [locfit package in R (Loader 1997)] is bimodal (Fig. 2a), with the modes centered at $T = 1.0$ and 2.8 K. Also, we show the quantile-quantile plot (basically the plot between the cummulative PDFs from the data and an assumed fitted distribution; Wilk and Gnana-desikan 1968) based on gamma distributions with the corresponding skewness and mean fitted to the observational data has a S-shape that is suggestive of bimodality (Wilk and Gnanadesikan 1968; Lee et al. 1998), with two approx-imately parallel straight segments corresponding to these modes (Fig. 2b). However, the "dip test" for multimodality (Hartigan 1985) produces a p value of 0.4, while the Sil-verman test for bimodality (Silverman 1981; Hall and York 2001) produces a p value of 0.17, indicating that we cannot conclusively demonstrate the bimodality in the observations. The main limitation for passing the test is that the strong EN are still too few compared to the moderate EN, but if in the coming years the strong 1982–83, 1997–98 and 2015–16 El Niño events were to repeat themselves, as well as other four moderate EN events, then we would get $p < 0.09$ from the dip test (i.e. passing at the 90% level).

The probability density function (PDF) for CTL is bimodal (Fig. 2), with the modes corresponding to the moderate and strong EN events peaking at 0.8 and 1.8 K,
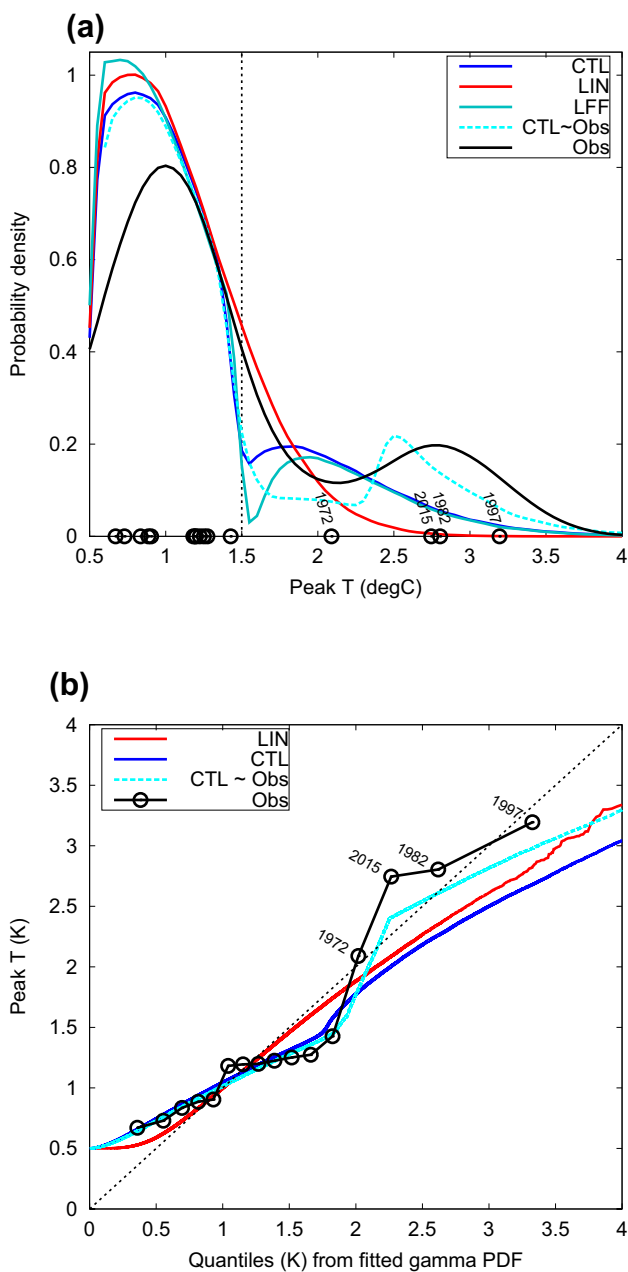
(a)

(b)

Fig. 2 **a** Estimated probability density functions (PDF) for the peak T during El Niño events. The smoothed PDF for observations was estimated using the locfit package in R, while the model PDFs based on binned histograms from 2 Myr data are shown for the linear model (LIN, red) and the control (CTL, blue). Also shown are the results for selected non-overlapping 67-year periods from the CTL (13.1% of the total 2 Myr) in which there are more peaks with $T > 2.4$ than between 1.6 and 2.4 (dashed cyan). **b** Quantile–quantile plots of the data in **a** against the correspondingly fitted gamma distributions

estimate could indicate limitations in the model, e.g. perhaps it should be unstable for $T > T_c$. But it seems more likely that this is associated with the shortness of the observational sample. If we sample the 2 Myr CTL run in non-overlapping time segments of the same length as the observational record (67 years) and search for those segments with the statistics of EN peaks similar to the observed (Fig. 2), specifically that they contain a larger number of EN peaks for $T > 2.5$ K than the number of peaks in the dip with $1.5 < T < 2.5$ K (such as the one in Figs. 3, 4), we find that 13% of the time segments satisfy this criterion. This is much less likely in LIN (1%).

The skewness of the distribution of EN T peaks in the nonlinear model (1.47) is larger than the observational value (1.11), whereas the linear model is lower (0.89). However, if we sample the model runs in time segments as long as in the observations, the 95% confidence intervals from the linear and nonlinear models ([− 0.19, 1.68] and [0.11, 2.33], respectively, for 10,000 subsamples) have substantial overlap, so the skewness from observations is not a useful statistic for discriminating between the two models.

4.2 Evolution of El Niño events and rectification of high-frequency forcing

The trajectories in T-h phase-space of the observed monthly T and h for the 1950–2016 period (Fig. 3a) are irregular orbits. However, as noted by Kessler (2002), occasionally strong EN appear as clockwise excursions that appear more deterministic: from positive h moving towards large positive T, with h starting to strongly decrease soon before the peak T, leading to the neutral to negative values of T. The extreme nature of the strong EN peaks has been previously characterized by large eastern Pacific warming (Takahashi et al. 2011; TD16), although the 2015–2016 event only presented about half of the warming near the South American coast than the warming during the 1982-1983 and 1997–1998 events (L'Heureux et al. 2016; Dewitte and Takahashi 2017). An important aspect of the onset of these observed strong EN events is that, in contrast to the "pure" (unforced) RD dynamics, in general h does not decrease as sharply when T increases towards its peak as afterwards, during EN decline; in 1982, h even increased right up to two months prior to the peak T. This indicates that, if the RD model is indeed representative of the underlying dynamics, the onset of the 1982 (and probably also the other) strong EN was strongly facilitated by external forcing (TD16). On the other hand, after the observed EN peaks, the pronounced discharge process leads to large negative h, but the associated La Niña peak T anomalies are not as large as the ones for the EN events in the Niño 3 region.

A representative 67-year segment from the nonlinear (CTL) model run is presented in Fig. 3c, showing that this model (but not the linear model in Fig. 3b) reproduces
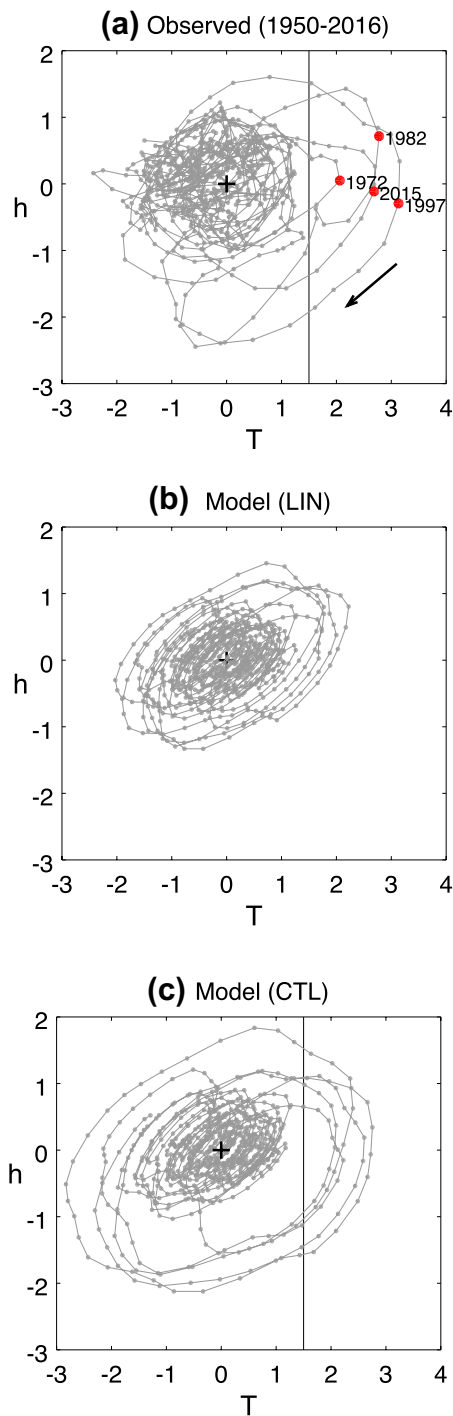
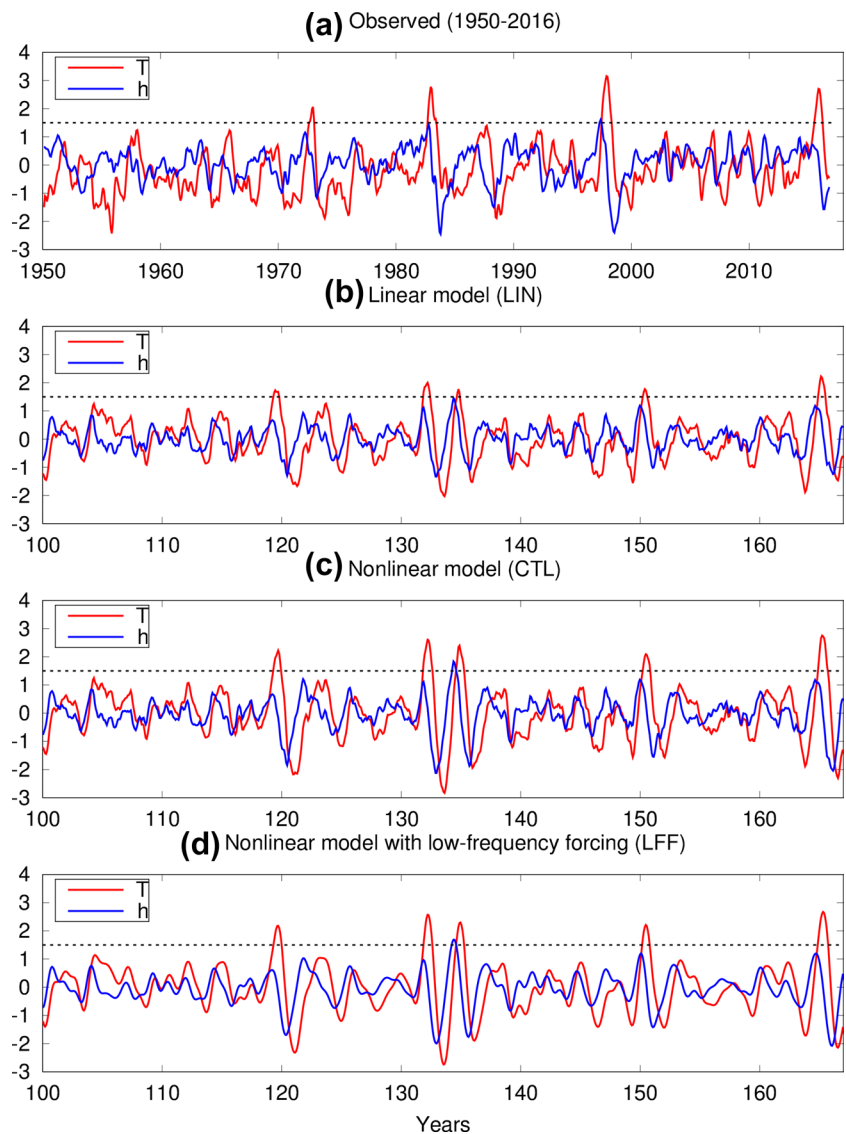respectively, while the in-between minimum is located slightly above $T_c = 1.5$ K. As expected, the PDF for LIN has no sign of bimodality.

The difference between the location and strength of the second mode in the PDF of CTL and the observational

Fig. 3 Monthly evolution of ENSO in *T-h* phase-space for **a** observations (1950–2016) and for a representative 67-year segment from the **b** linear (LIN) and **c** nonlinear (CTL) model runs (years 100–166). The data was smoothed with a 1–2–1 filter. The crosses indicate the origin, the dotted lines correspond to $T = 1.5$, and the arrow indicates the direction of the evolution of the strong El Niño events. In **a**, *T* is Niño 3 SST anomalies from ERSST v3b (Smith et al. 2008) and *h* is the combination of SODA 2.2.4 (1950–1979; Giese and Ray 2011) and GODAS (1980–2016; Behringer and Xue 2004) 120°E–80°W, 5° S–5°N 20 °C depth anomaly (removing the mean difference between the two products), with the December values for the largest El Niño events indicated with a red dot

both the excursions associated with the strong EN, as well as the muted discharge during their onset and the large discharge during and after the peak. However, our model overestimates the magnitude of the subsequent La Niña *T* anomalies through conventional RD dynamics, leading to the underestimation of the skewness of *T* (0.12, calculated over the full run) relative to the observed (0.71). This is probably a consequence of not considering the spatial asymmetry of El Niño and La Niña in our model, as the largest SST anomalies tend to be further to the west in the latter (e.g. Monahan and Dai 2004; Takahashi et al. 2011; Dommenget et al. 2012), lack of nonlinear damping of La Niña (e.g. DiNezio and Deser 2014; TD16) or lack of seasonality in the feedbacks (e.g. Stein et al. 2014). The thermocline feedback accounted for in the model through the parameter *b* also appears to have an asymmetry in nature (Dewitte and Perigaud 1996; An and Kim 2017) that is not taken into account in our model.

The time series of observed *T* and *h* (Fig. 4a) also illustrates how positive (but not necessarily large) *h* precedes the peak *T* associated with strong EN after which *h* becomes strongly negative and *T* drops, although not as much. The LIN and CTL models (Fig. 4b, c) also reproduce this behavior to a large extent, albeit overestimating the La Niña and the likelihood of a second strong EN afterwards. The robust characteristics of the temporal evolutions of the strong and moderate EN events are highlighted by the the spread among the individual EN events in *T* and *h* at different times (*t*) relative to the peak *T* (*t* = 0), which indicates that during the early part of the onset of strong EN events (between *t* = −10 and *t* = −6), both *T* and *h* are positive and increase together in observations and the model (Fig. 5a, c). After *t* = −6, *T* continues increasing but *h* decreases steeply, particularly around *t* = 0, reaching a minimum around *t* = 7. Meanwhile, *T* decreases from the peak at *t* = 0 through *t* = 12. This continues to *t* = 15 in the model, but not in observations, reaching lower values of *T* (stronger La Niña). Positive precursor *h* is a necessary condition for strong but not for moderate events, consistent with TD16, but there are many strong and moderate events that have the same initial *h*.

The series for LIN and CTL are remarkably similar (Fig. 4b, c), indicating that CTL is only weakly nonlinear and that stochastic forcing dominates the variability. As might be expected, the only differences between the two experiments appear after *T* exceeds $T_c = 1.5$ K, leading to larger EN peaks when $T > T_c$ in CTL (Fig. 6a; the slope of the scatterplot for $T > 1.5$ is 1.8), as well as stronger discharge and subsequent La Niña. We note that most of the strong events in CTL were also the strongest events in LIN (Fig. 6a). This also influences the results for a few years after a strong EN, associated with larger RD oscillations (Fig. 4b, c). Furthermore, the power spectra of *T* in the LIN and CTL (Fig. SM1) both have a single peak at almost the same

Fig. 4 Timeseries of T (red) and h (blue) from **a** observations (1950–2016), and from the **b** linear (LIN) and **c** nonlinear (CTL) model run (years 100–166)

(a) Observed (1950-2016)

(b) Linear model (LIN)

(c) Nonlinear model (CTL)

(d) Nonlinear model with low-frequency forcing (LFF)

Years

intrinsic frequency but, since the nonlinear system is less damped (i.e. more oscillatory), the spectral peak is stronger.

It has been emphasized before that the low-frequency component of the forcing is the most important factor driving ENSO (Roulston and Neelin 2000; Zavala-Garay et al. 2008; Levine and Jin 2010) and we find that this is also true of our CTL model, as the experiment with low-frequency forcing (LFF; Fig. 4d) produces a very similar (although smoother) ENSO evolution to the CTL run. Several studies indicate that high-frequency forcing (on intraseasonal scales) has a rectified effect on the longer ENSO time-scales (Blanke et al. 1997; Zhang et al. 2003; Zavala-Garay et al. 2008). Indeed, the nonlinearity introduces some rectification from high to low frequencies in our model, leading to a 4% increase from LFF to CTL in the power at the spectral peak corresponding to the ENSO period (Fig. SM1). The high-frequency forcing also increases the number of strong EN

events (peaking with $T > 1.5$; Fig. 6b) by 30.7%, although the total number of EN events was little affected (94% in LFF relative to CTL). This can be seen by comparing those cases in which the low-passed T from the CTL run is larger than in LFF (Fig. 7). In CTL, as T approaches T_c from below a positive pulse associated with the high-frequency forcing component at $t = -6$ (red line in Fig. 7) allows T to overcome T_c. This does not happen in LFF and as a result T stays below T_c. The weaker subsequent negative pulse cancels out with the low-frequency forcing and T continues growing through undamped RD dynamics.

Removing the high-frequency component (LFF) reduces the variance of the forcing to 16% of the original (CTL), but the variance of T is only reduced to 95%. This weak sensitivity is to be expected when forcing a damped (weakly nonlinear) oscillator far from its natural frequency. If we instead run the model with only the high-frequency (period
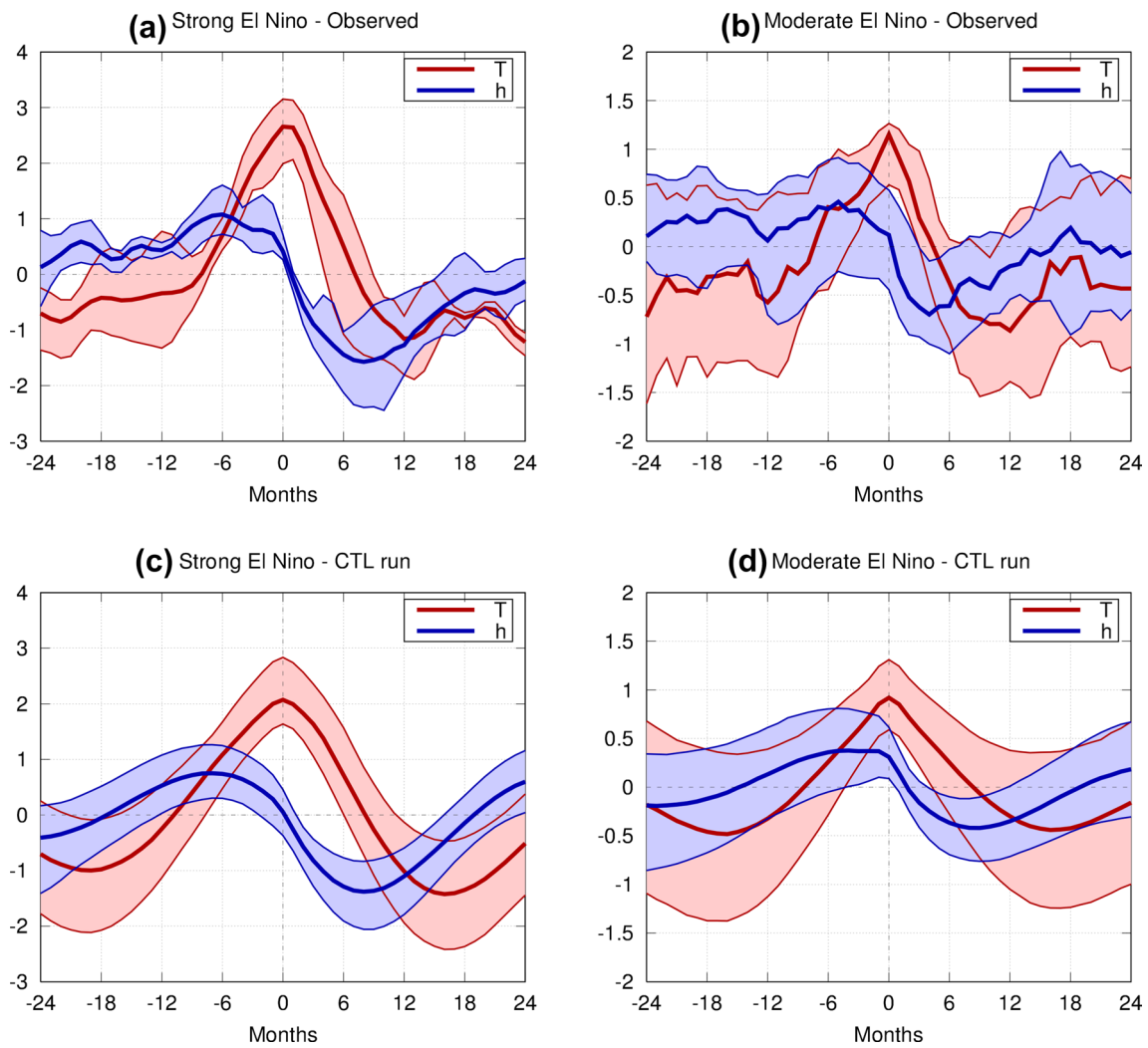
Fig. 5 **a**, **b** Observed and **c**, **d** modeled evolution of *T* (red) and *h* (blue) with respect to the peak *T* values of the **a**, **c** strong and **b**, **d** moderate El Niño events. The shaded range is between the 10 and 90-percentiles of the events, with the median shown with a thick line (except for the observed strong El Niño, for which the overall range and the mean are shown). A 1–2–1 filter was applied to all data

Fig. 6 Subsample of *T* at El Niño peaks in the nonlinear (CTL) run against the nearest peak *T* of the same events (no more than 3 months apart) in the **a** linear (LIN) run and **b** the nonlinear model with low-passed forcing (LFF)
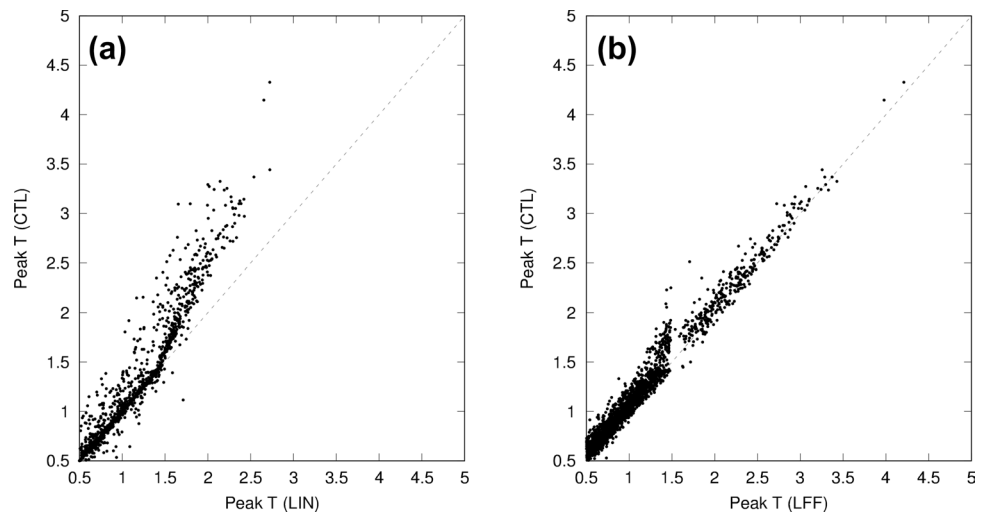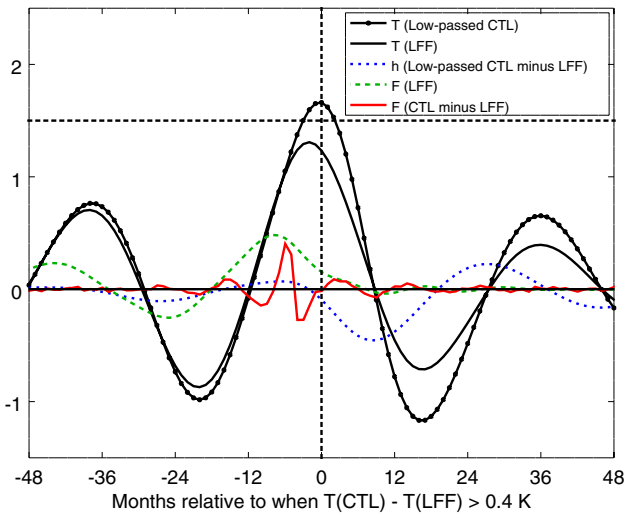
Fig. 7 Composite-mean temporal evolution in months relative to when the difference between the low-passed T from CTL and T from LFF is larger than 0.4 K (not necessarily EN events). T is shown in black (low-passed CTL solid with dots, LFF solid), the low-frequency (green dashed) and high-frequency (red solid, only for CTL) components of the forcing, as well as the difference in h between the low-passed CTL and the LFF runs (blue dotted)

< 1 year) forcing component (not shown), it produces a much weaker T variance (1% of CTL) and only in the high-frequency range. For very high-frequencies, the dynamics are those of a random walk ($dT/dt \approx F_0\xi$) rather than ENSORD dynamics.

4.3 Dynamics of El Niño events

For a 2D model such as ours, a phase portrait (Fig. 8) is a powerful tool for analyzing the dynamics, as the non-linearities and stochastic processes acquire a geometrical interpretation. The deterministic RD dynamics, i.e. the tendency terms that depend on T and h on the right hand side of Eq. (1), are represented by vectors in the T-h space (black arrows) tracing clockwise inward spirals, as expected from a damped oscillator. The nonlinear net feedback in CTL, i.e. a reduced damping of T for $T > T_c$, is manifested as a smaller component towards the left in these vectors for a given h relative to the LIN model (not shown). This might appear subtle in the tendencies (black vectors), but sample deterministic trajectories (green lines) starting from an ENSO neutral state ($T = 0$) with charged heat content ($h > 0$) show a substantial divergence around $T = T_c$, with those exceeding T_c having a weak decay of T, whereas those that stay below T_c follow a fast spiral towards the origin. Since all deterministic trajectories eventually decay towards the origin, the model is globally stable.

The actual evolution of the strong and moderate EN events is shown in Fig. 4 as time-series centered at the time
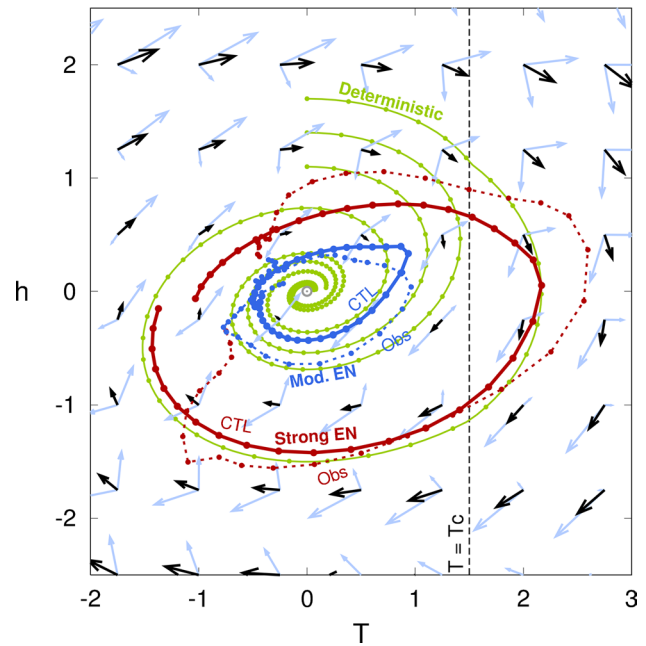

Fig. 8 Phase portrait of the nonlinear (CTL) model in $T - h$ space, showing the deterministic tendencies (black arrows), plus and minus twice the standard deviation of the external forcing (light blue arrows). Sample determininistic trajectories are shown in green. The composite mean trajectories of strong (red) and moderate (blue) El Niño events are also shown for the model (solid) and observations (dotted). Each dot corresponds to one month and all trajectories are clockwise

of the peak T. In phase-space, the average trajectories show a good correspondence between the observations and the model (Fig. 8) but, in both cases, they appear more "horizontal" during the onset of the EN events than the deterministic RD trajectories, i.e. have a larger growth in T and weaker decay in h. The departure from RD dynamics during the onset indicates an important role of the sustained favorable stochastic forcing over the course of around 9 months, from the charged and ENSO neutral state to slightly after when T exceeds T_c. In the CTL model, we set equal external forcing for T and h, so it acts along the diagonal in the phase-diagram (Fig. 8) and, when added to the deterministic tendency (black vectors), the net tendency vector (blue arrows) is deflected along that diagonal, depending on the sign and magnitude of the forcing. For a mean net tendency consistent with the onset of strong EN events, the forcing would need to have a mean positive value along 9 months or so. For a 9-month mean value of F of 0.1 or more, the probability of occurrence is 4% in CTL.

After the peak T is achieved, the EN events on average follow the deterministic trajectories towards a neutral T and negative h state. This should be expected a priori in the model, since our compositing procedure does not constrain the behavior of the forcing after the peak and the forcing

effect should average to zero. However, since this is also seen in the few cases in observations, it suggests that it is the large magnitude of the deterministic discharge of h associated with the high values of T (cT term in Eq. (1); see below) that dominates the decay of the strong EN.

The role of the forcing during the onset of the strong EN is also made evident by a more conventional "surface heat budget", i.e. analysis of the T tendency terms on the right hand side of Eq. (1), which shows that the warming contribution of the bh term and the direct effect of the forcing are comparable (the former somewhat larger) between approximately $t = -15$ and $t = 0$ (Fig. 9a). However, the positive value of h between $t = -10$ and $t = -1$ is itself also maintained primarily by the forcing against the opposing discharge mechanism (cT term), which grows as EN grows (Fig. 9b). Thus, it is the forcing that is ultimately responsible of the growth of EN during the year previous to its peak. A similar situation is observed for the moderate EN

events, but with a shorter time in which the forcing dominates the warming (after approximately $t = -10$; Fig. 9c, d). We should note that the fact that the stochastic forcing tends to be positive during the onset of EN does not indicate state-dependence, just that EN tends to occur after periods of randomly positive forcing. The nonlinearity in the $a_{NL}T$ term helps the growth of the strong EN by suppressing the damping after approximately $t = -4$ (Fig. 9a), which does not happen for the moderate EN (Fig. 9c).

In the experiment in which the forcing of T and h are uncorrelated (indepF), which has the same standard deviation of T as in CTL, the growth of T during strong and moderate EN is dominated by the bh term (Fig. SM2a, c), but h itself is sustained by the corresponding forcing against the discharge after $t = -10$ (Fig. SM2b, d), so effectively the growth of the EN event is sustantially aided by the forcing. In the experiment in which the forcing is only applied to T (FonlyT), which results in a standard
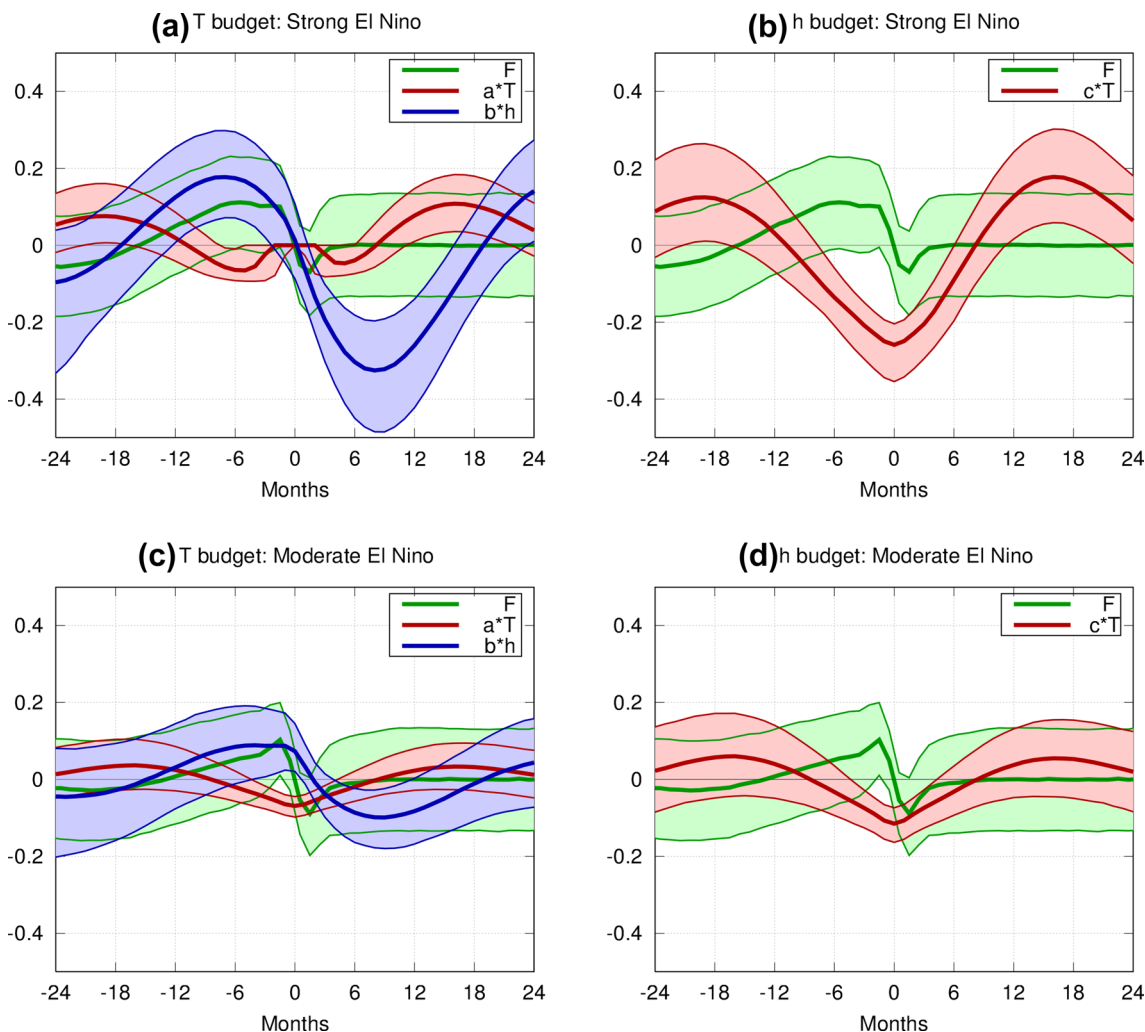

Fig. 9 Similar to Fig. 4 but for the tendency terms on the right hand side of Eq. 1 for **a**, **c** T ($a_{NL}T$ in red, bh in blue, and F in green) and for **b**, **d** h (cT in red, dh in blue, F in green) during **a**, **b** strong and **c**, **d** moderate El Niño events

deviation of T 24% larger than that of CTL, the warming contribution of bh again dominates the growth of T in both strong and moderate EN up to approximately $t = -4$, after which the forcing is dominant (Fig. SM3a, c). Since $dh/dt = cT$ in this last experiment (Fig. SM3b, d), T and h are in quadrature and do not exhibit joint growth during the onset of strong EN events that is seen in the previous experiment, in CTL and in observations.

The growth of EN events in our model stops when the positive forcing ends (with brief appearance of negative forcing in $t = 1$ to $t = 3$) and the bh term vanishes (Fig. 9a, c), after which the negative bh induced mainly by the deterministic discharge process (cT term; Fig. 9b, d) takes over and T decreases (Fig. 9a, c). The discharge after a strong EN is perhaps the most predictable aspect of ENSO in our model, as also suggested in more comprehensive models and observations (e.g. TD16). It should be noted that in nature, the seasonality of the ENSO feedbacks (e.g. Stein et al. 2014) sets the timing of the peak T, particularly the discharge term in boreal winter (Vecchi and Harrison 2006, 2006; McGregor et al. 2012).

4.4 Probability dynamics and the Fokker–Planck equation

To represent a possible situation of interest for real-time prediction, in Fig. 10 we used the Fokker–Planck Eq. (3) to simulate the evolution of a PDF corresponding to an ensemble initialized around a weak EN state that is strongly-charged (a gaussian PDF centered at $T = 0.6$ and $h = 1.0$ with a width scale of 0.1) for both the linear (LIN) and nonlinear (CTL) versions of our RD model. The results are very similar to those obtained by identifying the states in the 2 Myr CTL model run around $T = 0.6$ and $h = 1.0$ and looking at the evolution of the ensemble (not shown).

Within the first 3 months of the simulations, even though the mode of the PDF follows the deterministic dynamics and stays below T_c, both models show a large spread of the PDFs along the diagonal direction due to the stochastic forcing, producing around 10% probability of exceeding T_c (i.e. strong EN; Fig. 10). This probability continues to grow until month 7 in both cases but, in the nonlinear model, a second mode with $T > T_c$ appears shortly after month 6, leading to the bimodal distribution of EN peaks (Sect. 4.2). Due to the reduced damping, the probability of $T > T_c$ in the nonlinear
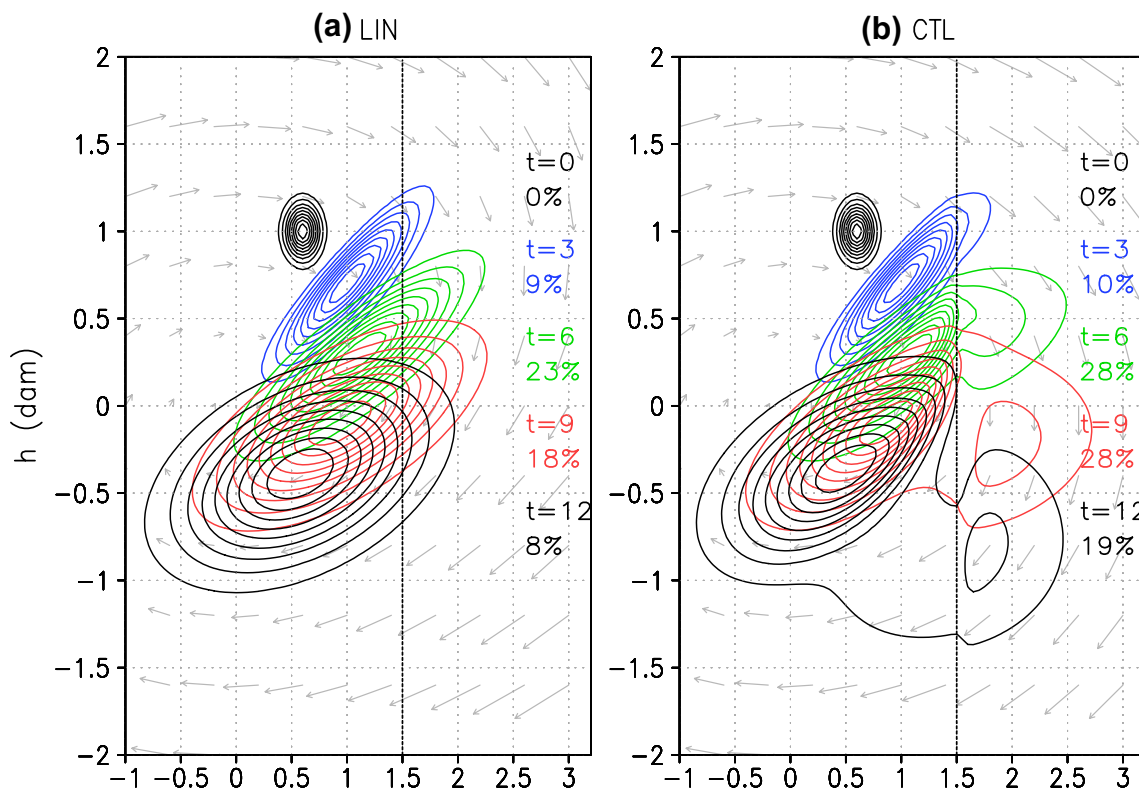

Fig. 10 Evolution of the joint T-h PDFs of an ensemble initially centered at $T = 0.6$, $h = 1.0$ (black), after 3 (blue), 6 (green), 9 (red), and 12 (black) months from the solution of the Fokker–Planck equation for the **a** linear and **b** nonlinear RD model. For visualization purposes, the PDFs were normalized by their peak value and contoured at 0.1–0.9 with an interval of 0.1. The deterministic tendencies are shown as grey arrows. The probability of $T > 1.5$ for the each time is indicated as %

model reaches higher values and decays slower than in the linear model.

The role of the regime-shift term in the formation of the bimodal PDF was assessed by setting its value to zero in Eq. (3) and solving numerically for the case above. As shown in Fig. 11, as in CTL, the marginal PDF for T (i.e. integrated in h) spreads to higher T than in the linear case due to larger positive drift (advection) for $T > T_c$, it does not develop a second mode. On the other hand, if we maintain the regime-shift term but we remove the differential advection by setting $a_{NL} = a$ for all T in the advection term, the positive tail of the PDF remains short, similar to the linear case, and develops a change in slope near $T = T_c$, but also not a second mode. This means that both the regime-shift
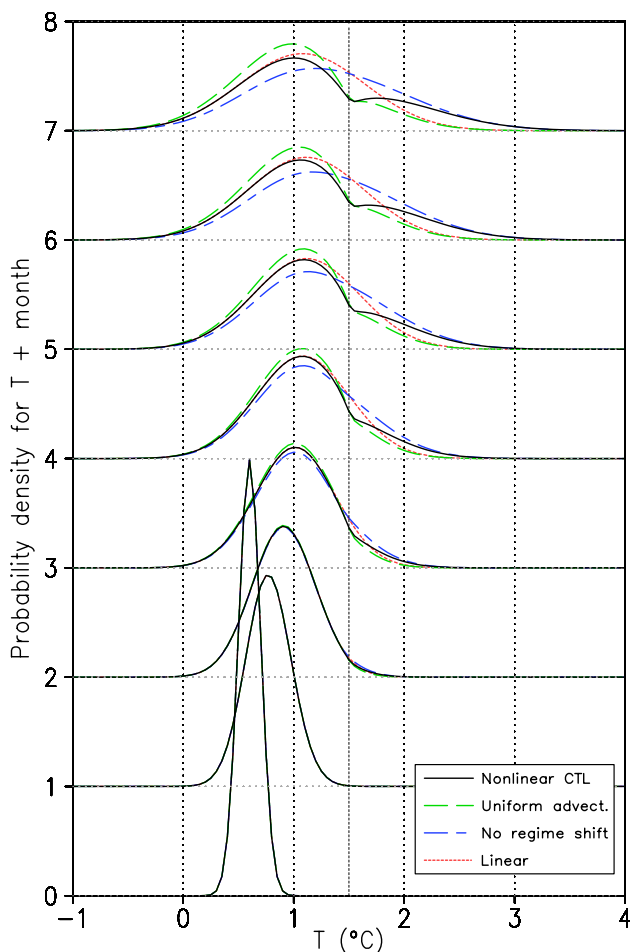

Fig. 11 Evolution of the marginal PDFs for T for the case in Fig. 10 for months between $t = 0$ and $t = 7$ (offset by the corresponding number of months) obtained from the Fokker–Planck equation for the linear (red dotted) and nonlinear (solid black) model. Also shown for experiments in which (1) the $d(a_{NL})/dT$ was set to zero in the Fokker–Planck equation (blue short-long lines) and in which (2) the $d(a_{NL})/dT$ term was retained but a_{NL} was set to a for $T > T_c$ (green long lines). In these two non-conservative experiments, the PDFs were renormalized so that the total probability is 1

term and the differential advection are necessary to generate and to separate the two modes of the PDF. For the two modes to develop it is not essential that a_{NL} is discontinuous: an experiment with a hyperbolic tangent formulation for a_{NL} with an exponential scale for T of 0.2 produces similar results (not shown).

If we consider the equilibrium probability density ρ calculated from the Fokker–Planck Eq. (3) for positive T for $h = 0$, which approximately corresponds to the peak T during EN (e.g. Fig. 5), we can also see the bimodality associated with T (grey contours in Fig. 12), which becomes more pronounced for $h < 0$. The analysis of the terms of the steady-state F-P equation (shading in Fig. 12) provides an approximate condition for this bimodality. The antinode or dip is found around $T = T_c$ for $h \le 0$, where we find the main balance between the diffusion term (Fig. 12d) and the "regime shift" term (Fig. 12f), so the approximate steady-state F–P Eq. (3) near the antinode is:

$$0 \approx -\frac{da_{NL}}{dT} T\rho + F_0^2 \frac{\partial^2 \rho}{\partial \phi^2}.$$

The diffusion term is negative because it is dominated by having an antinode in ρ along T (i.e. $\partial^2 \rho / \partial T^2 > 0$). Since $\rho > 0$, while $T > 0$ for El Niño, this balance can only be possible for:

$$\frac{da_{NL}}{dT} > 0,$$

which is the source of the bimodality in our nonlinear RD model.

Although it seems plausible that multiplicative forcing could also produce bimodality, when we introduced it by enhancing the amplitude of the forcing for $T > T_c$ in the linear model (MULTLIN), it did not produce a bimodal distribution (Fig. SM4). Furthermore, in the nonlinear model (MULT) it produced a less pronounced second mode in the PDF (Fig. SM4). We can understand this in the context of the Fokker–Planck equation, as the enhancement of the stochastic forcing with T implies an enhancement of the diffusion, which flattens the PDFs and increases the positive tail. Additionally, it introduces a term of the form $-(\partial G / \partial T)\partial \rho / \partial T$ ($G \equiv [1 + BH(T - T_c)(T - T_c)]$), which near $T = T_c$ behaves similarly to the $-(a_{NL}T)\partial \rho / \partial T$ term, producing a divergence in the drift that advects ρ. However, this multiplicative forcing does not produce a "regime-shift" term equivalent to $-(da_{NL}/dT)T\rho$, which we found above to also be necessary to generate the bimodality.

The relatively short adjustment time of the spread is important for predictability. In the simpler stochastic climate model consisting of a slab ocean layer forced by weather noise (Frankignoul and Hasselmann 1977), the equation has the form $dT/dt = aT + F_0\varepsilon(t)$ (a Langevin
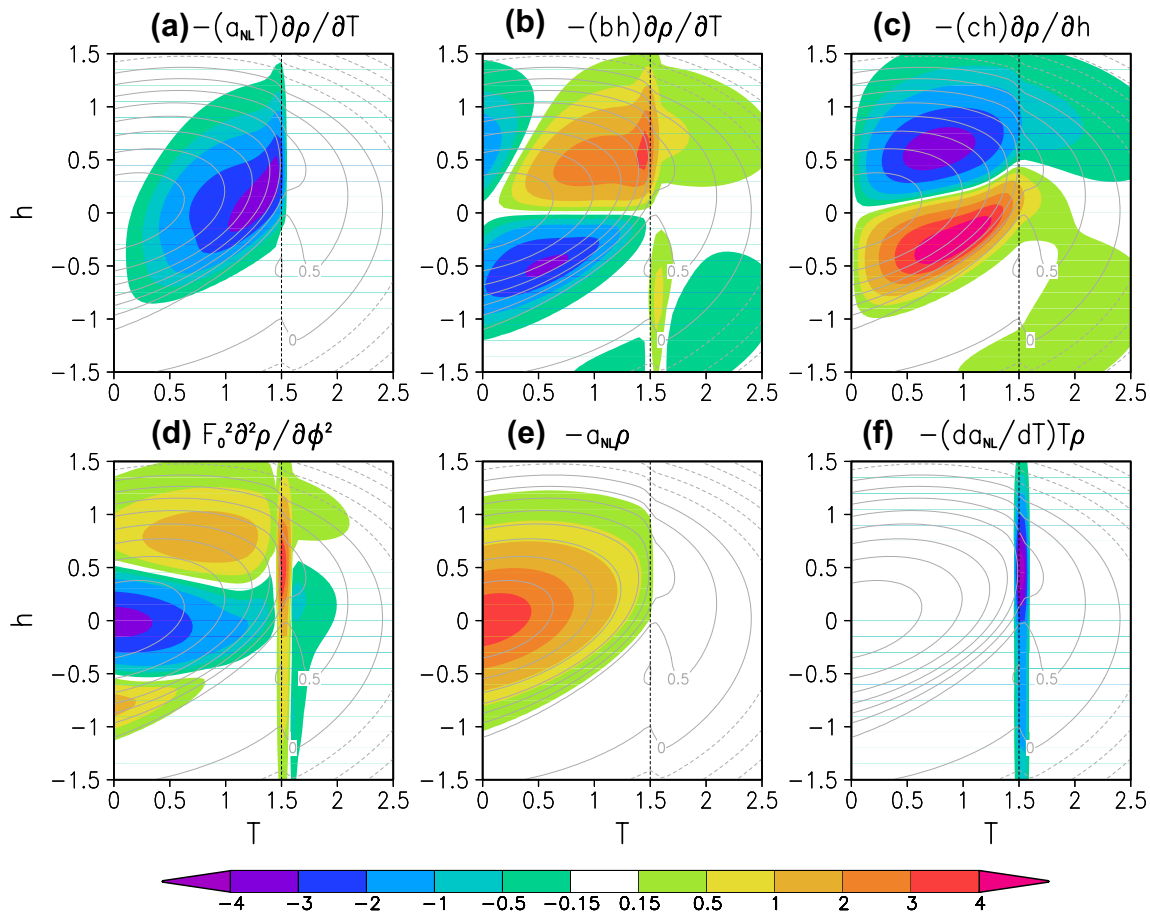
Fig. 12 Equilibrium probability density (grey contours; shown as $\log(100\rho)$) from the steady-state Fokker–Planck Eq. (3) for the CTL model and the different equation terms (K^{-1} dam^{-1} month^{-1}): the advection terms along the T direction **a** $-(a_{NL}T)\partial\rho/\partial T$ and **b** $-(bh)\partial\rho/\partial T$, **c** the advection term along the h direction $-(cT)\partial\rho/\partial h$, **d** the diffusion term due to the stochastic forcing $F_0^2\partial^2\rho/\partial\phi^2$, **e** the damping term $-a_{NL}\rho$ and **f** the regime shift" term $(da_{NL})/dT)T\rho$. The dashed line indicates $T = T_c$

equation), and the ensemble variance σ_T^2 adjusts exponentially to its equilibrium value $F_0^2/|2a|$ with a timescale $|2a|^{-1}$ (Hasselmann 1976). In our model, we analyzed the adjustment of the variance of T from the delta-like initial PDF used above but centered at different points in the $T > 0.2$, $h > 0.2$ quadrant, most relevant for EN development. In the linear case the adjustment of the variance to its equilibrium value is the same for all initial points (we also tested other quadrants) and oscillates due to the rotation of the elliptically-elongated PDF induced by the drift. The rotation leads to increased variance when the PDF is more oriented in the T direction, approximately every half period. The adjustment is within the range of exponential adjustment functions with timescales $|2a|^{-1}$ and $|a|^{-1}$, and shows the sharpest increase within the first year (Fig. SM5a). For the nonlinear model, the oscillations are similar but with phase-shifts and with larger amplitudes for larger initial h and T, with the former having a larger

impact Fig. SM5b). Again, the largest increase is seen in the first year. During the first 6 months the adjustment is bounded by the exponential timescales $|2a|^{-1}$ and $|a|^{-1}$. We observe that the influence of the initial conditions on the variance persists for almost 10 years, with larger variance associated with the second mode of the PDF (strong EN). Interestingly, if the stochastic forcing of T and h are uncorrelated (i.e. the diffusion term in Eq. (3) is given by $0.5F_0^2(\partial_T^2 + \partial_h^2)\rho$), then not only the oscillations are greatly reduced but the adjustment follows closely the $|a|^{-1}$ exponential decay (not shown).

To assess how the equilibrium variance of T scales with a, we performed 2 Myr runs of the linear and nonlinear RD models with different values of a and fixed forcing amplitude ($F_0 = 0.17$). We found that, for the linear model, the variance scales with $|a|^{-1}$ (not shown), just as for the slab ocean model. However, for the nonlinear model, the variance scales as $|a|^{-1.25}$. The goodness of fit is somewhat surprising considering that in the nonlinear model the damping a_{NL} is

not constant, so it should not be considered a strict scaling. Still, the dependence of both the timescale and equilibrium variance with the damping could provide a useful framework for interpreting the ensemble spread in ENSO predictions.

5 Discussion

The formulation of our model has been guided by the objective of providing the simplest explanation for the EN regimes. Thus, we ensured that the nonlinearity does not produce unstable growth, only suppresses the damping. Therefore, this model does not produce self-sustaining nonlinear oscillations that would require nonlinear damping or that could produce multiple equilibria that includes a permanent EN state, which is questionable in theoretical model settings (Neelin and Dijkstra 1995). Despite the simplicity of our model, we have found that it adequately reproduces the evolution of T and h of the strongest observed EN events and the bimodal distribution, so it provides a parsimonious theory for EN regimes.

The level of agreement between the bimodal probability distributions of El Niño peaks in the model and in the observational record (Sect. 4.2) is affected by two factors: (1) the adequacy of the model to reproduce the essential dynamics of the true system, and (2) the adequacy of the observational record to provide a representative sample of the behaviour of the true system. Validation of model behaviour is inevitably done by comparison to the available observations, which implicitly assumes that the observations are more reliable than the model and tends to lead to fitting the model to such observations. A different and complementary approach is the validation of model processes, which can be expected to be better constrained by short records if we assume uniformitarianism, i.e. that the essential physical processes that are observed now are also valid in unobserved periods. In our model, adding the nonlinear Bjerknes feedback with a critical temperature of around 27.5 °C did not involve fitting the statistics of El Niño peaks, so the result that only 13% of the periods are similar to the observational one is an emergent result. In the hypothetical case that our model captured the essential dynamics associated with of the long term variability of ENSO, our results would imply that our observational record could be inadequate for characterizing the statistics of the true system (cf. Wittenberg 2009), so we argue that the assessment of the physical processes is probably more important than fine-tuning models to the statistics from the observational record.

Karamperidou et al. (2016) showed that the nonlinearity in the PC1–PC2 phase space can be related to the balance of linear ENSO feedbacks in CMIP5 simulations, in particular to the strength of thermodynamical damping in the eastern Pacific. However, we have not attempted to observationally constrain the values of a_{NL} for T above or below T_c. The calculation of the parameters for the nonlinear net feedback on T from first principles would require adapting a methodology such as the BJ index (Jin et al. 2006) to the nonlinear case. Although TD16 found that the zonal wind response to the surface eastern Pacific warming is enhanced by a factor of 3 and cloud nonlinearity results in a change in the sign of the feedback (Lloyd et al. 2012a), the effective Bjerknes feedback also includes how the ocean currents, thermocline, and upwelling respond to the warming. Perhaps other empirical methods (e.g. Burgers et al. 2005) could be adapted to consider this nonlinearity, or the proposed model could be used to derive an estimate of the non-linear feedback through assimilation of observations.

This model highlights the key role of the stochastic forcing, particularly the component of the forcing on ENSO time-scales, in the growth of the strong EN events (e.g. Levine and Jin 2010; TD16). It is often assumed that the low-frequency positive forcing is the result of clustering of short-term westerly wind events, either randomly or modulated by SST (e.g. Gebbie et al. 2007; Zavala-Garay et al. 2008; Gebbie and Tziperman 2009). However, intrinsically low-frequency forcing processes associated with equatorial westerly wind anomalies also exist, such as the seasonal footprinting mechanism (Vimont et al. 2001, 2003) and the Pacific Meridional Mode (Chang et al. 2007; Larson and Kirtman 2013) based on the North Pacific, the South Pacific meridional mode (Zhang et al. 2014), propagating signals from the Indian Ocean (Clarke and Gorder 2003; Izumo et al. 2010), the southerly wind to the east of Australia (Harrison 1984; Hong et al. 2014) and the precursor warming in the far-east Pacific (Takahashi and Martínez 2016; Dewitte and Takahashi 2017).

The strong La Niña following strong EN events in our nonlinear model is consistent with the strong heat content discharge that is seen in observations, except that in observations the discharge does not necessarily produce strong La Niña events. However, this model behavior is consistent with several GCMs (Cai et al. 2015; TD16) and could be indicative of missing physics, such as the nonlinearity in oceanic vertical thermal advection in the central Pacific (Dewitte and Perigaud 1996), particularly the saturation of vertical advection during La Niña (DiNezio and Deser 2014). Other potential processes could be the larger efficiency of the momentum flux in forcing equatorial waves in the western central Pacific during the onset of El Niño owing to the shallower thermocline (and enhanced stratification) associated to the tilt mode (Dewitte et al. 2013; An and Kim 2017). There is also an asymmetry of the thermocline feedback in the eastern Pacific since during La Niña events the shallowing thermocline can intersect the mixed layer, which is not the case during El Niño (note that this also explains the difference in

spatial pattern between strong EN and LN events (LN events having their peak anomaly more to the west).

6 Conclusions

The 2015–16 El Niño (EN) event provides a new data point consistent with the sparse strong EN regime and provides further observational evidence for the existence of strong and moderate EN regimes. However, it is not enough to statistically reject the null hypothesis of a unimodal distribution based on observations alone according to the tests considered.

On the other hand, as shown in a previous study (Takahashi and Dewitte 2016), the convective SST threshold in the eastern Pacific and the associated nonlinearity in the Bjerknes feedback provides a parsimonious explanation for this, motivating further exploration of this possibility suggestive with a simple theoretical model based on this mechanism.

Specifically, we modified the linear damped recharge-discharge ENSO model so that, above a threshold SST value, the net negative feedback is set to zero. Despite this nonlinearity, the model is stable and requires stochastic forcing in order to maintain the variability against the damping. Nevertheless, we show that this nonlinearity is sufficient to produce the bimodal distribution associated with strong and moderate EN regimes.

In this model, the growth of strong EN events is substantially contributed to by the low-frequency (periods greater than 1 year) component of the forcing, both by directly increasing T but also by maintaining the heat content h against the discharge process. The high-frequency component of the forcing helps some EN events to become strong (exceed T_c), leading to an overall increase of 31% in the number of strong events.

Due to the weak nonlinearity, the error growth associated with initial conditions is generally much smaller than the action of the stochastic forcing, so the evolution of the probability of ensembles of states is well described by the Fokker–Planck equation. The ensemble spread adjusts towards an equilibrium value that depends on the damping in the model, with the adjustment occurring in the damping timescale as well, leading to a fast growth of the spread within the first year. This helps part of the probability distribution to exceed T_c and this part then becomes separated from the rest by a larger positive T tendency, leading to the bimodal EN distribution.

Our model is simple not only in that it adds only one free parameter to the original recharge-discharge model, namely the threshold temperature T_c, but also in that its behavior in many aspects does not depart much from the linear model. Thus, it is a parsimonious theory for the EN regimes, based on a well-known nonlinear SST-convection relation. It is a simpler model than, for instance, high-dimensional linear models and does not produce exotic behavior as other nonlinear models or require special assumptions about the forcing, thus providing a better null hypothesis for models that exhibit two EN regimes. This model could be fit to GCMs, either empirically or through physics-based approaches such as the BJ index (Jin et al. 2006) but adapted to the nonlinear situation proposed here, and serve as a diagnostic tool for interpreting, for example, long term variability in ENSO or the effects of climate change.

References

An SI (2008) Interannual variations of the tropical ocean instability wave and ENSO. J Clim. https://doi.org/10.1175/2008JCLI1701.1

An SI, Jin FF (2004) Nonlinearity and asymmetry of ENSO. J Clim 17:2399–2412

An SI, Kim JW (2017) Role of nonlinear ocean dynamic response to wind on the asymmetrical transition of El Nino and La Nina. Geophys Res Lett 44:393–400. https://doi.org/10.1002/2016GL071971

Ashok K, Behera SK, Rao SA, Weng H, Yamagata T (2007) El Niño Modoki and its possible teleconnection. J Geophys Res 112 (C11). https://doi.org/10.1029/2006JC003798

Battisti DS, Hirst AC (1989) Interannual variability in a tropical atmosphere–ocean model: Influence of the basic state, ocean geometry and nonlinearity. J Atmos Sci 46(12):1687–1712

Bellenger H, Guilyardi E, Leloup J, Lengaigne M, Vialard J (2014) ENSO representation in climate models: from CMIP3 to CMIP5. Clim Dyn. https://doi.org/10.1007/s00382-013-1783-z

Behringer DW, Xue Y (2004) Evaluation of the global ocean data assimilation system at NCEP: the Pacific Ocean. In: Eighth Symposium on Integrated Observing and Assimilation Systems for Atmosphere, Oceans, and Land Surface, AMS 84th Annual Meeting, pp 11–15

Blanke B, Neelin JD, Gutzler D (1997) Estimating the effect of stochastic wind stress forcing on ENSO irregularity. J Clim 10:1473–1486

Burgers G, Jin FF, van Oldenborgh GJ (2005) The simplest ENSO recharge oscillator. Geophys Res Lett. https://doi.org/10.1029/2005GL02295

Cai W, Wang G, Santoso A, McPhaden MJ, Wu L, Jin FF, Timmermann A, Collins M, Vecchi G, Lengaigne M, England M, Dommenget D, Takahashi K, Guilyardi E (2015) Increased frequency of extreme La Niña events under greenhouse warming. Nat Clim Change. https://doi.org/10.1038/nclimate2492

Capotondi A, Wittenberg AT, Newman M, Di Lorenzo E, Yu JY, Braconnot P, Cole P, Dewitte B, Giese B, Guilyardi E, Jin FF,

Karnauskas K, Kirtman B, Lee T, Schneider N, Xue Y, Yeh SW (2015) Understanding ENSO diversity. Bull Am Meteor Soc. https://doi.org/10.1175/BAMS-D-13-00117.1

Chang P, Zhang L, Saravanan R, Vimont DJ, Chiang JCH, Ji L, Seidel H, Tippet MK (2007) Pacific meridional mode and El Niño-Southern Oscillation. Geophys Res Lett 34:L16608

Chen C, Cane MA, Henderson N, Lee D, Chapman D, Kondrashov D, Chekroun MD (2016) Diversity, nonlinearity, seasonality, and memory effect in ENSO simulation and prediction using empirical model reduction. J Clim. https://doi.org/10.1175/JCLI-D-15-0372.1

Choi K, Vecchi GA, Wittenberg A (2013) ENSO transition, duration, and amplitude asymmetries: Role of the nonlinear wind stress coupling in a conceptual model. J Clim. https://doi.org/10.1175/JCLI-D-13-00045.1

Choi K, Vecchi GA, Wittenberg A (2015) Nonlinear zonal wind response to ENSO in the CMIP5 models: roles of the zonal and meridional shift of the ITCZ/SPCZ and the simulated climatological precipitation. J Clim. https://doi.org/10.1175/JCLI-D-13-00045.1

Clarke AJ, Van Gorder S (2003) Improving El Niño prediction using a space–time integration of Indo-Pacific winds and equatorial Pacific upper ocean heat content. Geophys Res Lett. https://doi.org/10.1029/2002GL016673

Dewitte B, Perigaud C (1996) El Niño-La Niña events simulated with Cane and Zebiak's model and observed with satellite or in situ data. Part II: Model forced with observations. J Clim 9:1188–1207

Dewitte B, Yeh S, Thual S (2013) Reinterpreting the thermocline feedback in the western-central equatorial Pacific and its relationship with the ENSO modulations. Clim Dyn. https://doi.org/10.1007/s00382-012-1504-z

Dewitte B, Takahashi K (2017) Diversity of moderate El Niño events evolution: role of air–sea interactions in the eastern tropical Pacific. Clim Dyn. https://doi.org/10.1007/s00382-017-4051-9

DiNezio PN, Deser C (2014) Nonlinear controls on the persistence of La Niña. J Clim. https://doi.org/10.1175/JCLI-D-14-00033.1

Dommenget D, Bayr T, Frauen C (2012) Analysis of the non-linearity in the pattern and time evolution of El Niño southern oscillation. Clim Dyn. https://doi.org/10.1007/s00382-012-1475-0

Eisenman I, Yu L, Tziperman E (2005) Westerly wind bursts: ENSO's tail rather than the dog? J Clim 18:5224–5238. https://doi.org/10.1175/JCLI3588.1

Frankignoul C, Hasselmann K (1977) Stochastic climate models, Part II Application to sea-surface temperature anomalies and thermocline variability. Tellus 29:289–305

Frauen C, Dommenget D (2010) El Niño and La Niña amplitude asymmetry caused by atmospheric feedbacks. Geophys Res Lett. https://doi.org/10.1029/2010GL044444

Gebbie G, Eisenman I, Wittenberg A, Tziperman E (2007) Modulation of westerly wind bursts by sea surface temperature: a semistochastic feedback for ENSO. J Atmos Sci. https://doi.org/10.1175/JAS4029.1

Gebbie G, Tziperman E (2009) Predictability of SST-modulated westerly wind bursts. J Clim. https://doi.org/10.1175/2009JCLI2516.1

Gerstner W, Kistler W (2002) Spiking neuron models. Single Neurons, Populations, Plasticity, Cambridge, p 480

Giese B, Ray S (2011) El Niño variability in simple ocean data assimilation (SODA), 18712008. J Geophys Res. https://doi.org/10.1029/2010JC006695

Graham NE, Barnett TP (1987) Sea surface temperature, surface wind divergence, and convection over tropical oceans. Science 238(4827):657–659

Hall P, York M (2001) On the calibration of Silverman's test for multimodality. Stat Sin 11(2):515536

Harrison DE (1984) The appearance of sustained equatorial surface westerlies during the 1982 Pacific warm event. Science 224:1099–1102

Hartigan PM (1985) Algorithm AS 217: computation of the dip statistic to test for unimodality. Appl Stat 35(3):320–325

Hasselmann K (1976) Stochastic climate models. Part I. Theory. Tellus 28:473–485

Hong LC, Ho L, Jin FF (2014) A Southern Hemisphere booster of super El Niño. Geophys Res Lett. https://doi.org/10.1002/2014GL059370

Izumo T, Vialard J, Lengaigne M, Montegut CdB, Behera SK, Luo JJ, Cravatte S, Masson S, Yamagata T (2010) Influence of the state of the Indian Ocean Dipole on the following year's El Niño. Nat Geosci. https://doi.org/10.1038/ngeo760

Jekabsons, G (2013) ARESLab: adaptive regression splines toolbox for Matlab/Octave v. 1.5.1, Reference Manual

Jin FF (1997) An equatorial ocean recharge paradigm for ENSO. Part I: Conceptual model. J Atmos Sci 54:811–829

Jin FF, Kim ST, Bejarano L (2006) A coupled-stability index for ENSO. Geophys Res Lett. https://doi.org/10.1029/2006GL027221

Karamperidou C, Cane MA, Lall U, Wittenberg A (2013) Intrinsic modulation of ENSO predictability viewed through a local Lyapunov lens. Clim Dyn. https://doi.org/10.1007/s00382-013-1759-z

Karamperidou C, Jin F-F, Conroy J (2016) The importance of ENSO nonlinearities in tropical Pacific response to external forcing. Clim Dyn. https://doi.org/10.1007/s00382-016-3475-y

Kessler WS (2002) Is ENSO a cycle or a series of events? Geophys Res Lett. https://doi.org/10.1029/2002GL015924

Kug JS, Jin FF, An SI (2009) Two types of El Niño events: cold tongue El Niño and warm pool El Niño. J Clim. https://doi.org/10.1175/2008JCLI2624.1

Larson S, Kirtman B (2013) The Pacific Meridional Mode as a trigger for ENSO in a high-resolution coupled model. Geophys Res Lett. https://doi.org/10.1002/grl.50571

Larkin NK, Harrison DE (2005) Global seasonal temperature and precipitation anomalies during El Niño autumn and winter. Geophys Res Lett 32:L16705

Levine AFZ, Jin FF (2010) Noise-induced instability in the ENSO recharge oscillator. J Clim. https://doi.org/10.1175/2009JAS3213.1

Lee J-Y, Woo J-S, Rhee S-W (1998) A transformed quantile-quantile plot for normal and bimodal distributions. J Inf Optim Sci 19(3):305–318

Levine AFZ, Jin FF (2017) A simple approach to quantifying the noise ENSO interaction. Part I: deducing the state-dependency of the windstress forcing using monthly mean data. Clim Dyn. https://doi.org/10.1007/s00382-015-2748-1

Levine AFZ, Jin FF, McPhaden MJ (2016) Extreme noise-extreme El Niño: How state-dependent noise forcing creates El Niño-La Niña asymmetry. J Clim. https://doi.org/10.1175/JCLI-D-16-0091.1

L'Heureux M, Takahashi K, Watkins AB, Barnston AG, Becker EJ, Di Liberto TE, Gamble F, Gottschalck J, Halpert MS, Huang B, Mosquera-Vásquez A, Wittenberg AT (2016) Observing and predicting the 2015–16 El Niño. Bull Am Meteor Soc. https://doi.org/10.1175/BAMS-D-16-0009.1

Lloyd J, Guilyardi E, Weller H (2012) The role of atmosphere feedbacks during ENSO in the CMIP3 models. Part III. The shortwave flux feedback. J Clim. https://doi.org/10.1175/JCLI-D-11-00178.1

Lloyd J, Guilyardi E, Weller H (2012) Local regression and likelihood. Statistics and computing series, vol 290. Springer, Berlin, p 1

Loader C (1997) Locfit: an introduction. Stat Comput Graph Newsl 8:11–17

McGregor S, Ramesh N, Spence P, England MH, McPhaden MJ, Santoso A (2012) Meridional movement of wind anomalies during ENSO events and their role in event termination. Geophys Res Lett. https://doi.org/10.1002/grl.50136

McGregor S, Timmermann A, Jin FF, Kessler WS (2015) Charging El Niño with off-equatorial westerly wind events. Clim Dyn. https://doi.org/10.1007/s00382-015-2891-8

McPhaden MJ, Busalacchi AJ, Cheney R, Donguy JR, Gage KS, Halpern D, Ji M, JulianP Meyers G, Mitchum GT, Niiler PP, Picaut J, Reynolds RW, Smith N, Takeuchi K (1998) The tropical ocean global atmosphere observing system: a decade of progress. J Geophys Res Oceans 103(C7):14169–14240

Monahan A, Dai A (2004) The spatial and temporal structure of ENSO nonlinearity. J Clim 17(15):3026–3036

Neelin JD, Dijkstra HA (1995) Ocean–atmosphere interaction and the tropical climatology. Part I: The dangers of flux correction. J Clim 8:1325–1342

Newman M, Shin SI, Alexander MA (2011) Natural variation in ENSO flavors. Geophys Res Lett. https://doi.org/10.1029/2011GL047658

Palmer TN (1993) Extended-range atmospheric prediction and the Lorenz model. Bull Am Meteor Soc 74(1):49–65

Rayner NA, Parker DE, Horton EB, Folland CK, Alexander LV, Rowell DP, Kent EC, Kaplan A (2003) Global analyses of sea surface temperature, sea ice, and night marine air temperature since the late nineteenth century. J Geophys Res 108(D14):4407. https://doi.org/10.1029/2002JD002670

Risken H (1996) The Fokker–Planck equation. Methods of Solution and applications, 3rd edn. Springer, Berlin

Roulston MS, Neelin JD (2000) The response of an ENSO model to climate noise, weather noise and intraseasonal forcing. Geophys Res Lett 27(22):3723–3726

Silverman BW (1981) Using kernel density estimates to investigate multimodality. J R Stat Soc B 43(1):9799

Su J, Zhang R, Li T, Rong X, Kug JS, Hong C (2010) Causes of the El Niño and La Niña amplitude asymmetry in the equatorial eastern Pacific. J Clim. https://doi.org/10.1175/2009JCLI2894.1

Suarez M, Schopf PS (1988) A delayed action oscillator for ENSO. J Atmos Sci 45(21):3283–3287

Smith TM, Reynolds RW, Peterson TC, Lawrimore J (2008) Improvements to NOAA's historical merged land–ocean surface temperature analysis (18802006). J Clim 21:22832296. https://doi.org/10.1175/2007JCLI2100.1

Stein K, Timmermann A, Schneider N, Jin F, Stuecker M (2014) ENSO seasonal synchronization theory. J Clim. https://doi.org/10.1175/JCLI-D-13-00525.1

Takahashi K, Montecinos A, Goubanova K, Dewitte B (2011) ENSO regimes: Reinterpreting the canonical and Modoki El Niño. Geophys Res Lett. https://doi.org/10.1029/2011GL047364

Takahashi K, Dewitte B (2016) Strong and moderate nonlinear El Niño regimes. Clim Dyn. https://doi.org/10.1007/s00382-015-2665-3

Takahashi K, Martínez AG (2016) The very strong El Niño in 1925 in the far-eastern Pacific. Submitted to Clim Dyn

Timmermann A, Jin FF, Abshagen J (2003) A nonlinear theory for El Niño bursting. J Clim 60:152–165

Vecchi GA, Harrison DE (2006) The termination of the 1997–98 El Niño. Part I: Mechanisms of oceanic change. J Clim 60:152–165

Vimont DJ, Battisti DS, Hirst AC (2001) Footprinting: a seasonal connection between the tropics and mid-latitudes. Geophys Res Lett 28(20):3923–3926

Vimont DJ, Wallace JM, Battisti DS (2003) The seasonal footprinting mechanism in the Pacific: Implications for ENSO*. J Clim 16(16):2668–2675

Wilk MB, Gnanadesikan R (1968) Probability plotting methods for the analysis for the analysis of data. Biometrika 55(1):1–17

Wittenberg A (2009) Are historical records sufficient to constrain ENSO simulations? Geophys Res Lett. https://doi.org/10.1029/2009GL038710

Zavala-Garay J, Zhang C, Moore AM, Wittenberg AT, Harrison MJ, Rosati A, Vialard J, Kleeman R (2008) Sensitivity of hybrid ENSO models to unresolved atmospheric variability. J Clim 21(15):3704–3721

Zhang L, Flügel M, Chang P (2003) Testing the stochastic mechanism for low-frequency variations in ENSO predictability. Geophys Res Lett 30:1630

Zhang H, Clement A, Di Nezio P (2014) The South Pacific meridional mode: a mechanism for ENSO-like variability. J Clim. https://doi.org/10.1175/JCLI-D-13-00082.1

Affiliations

Ken Takahashi[1] · Christina Karamperidou[2] · Boris Dewitte[3,4,5]

[1] Instituto Geofísico del Perú, Calle Badajoz 196, Mayorazgo IV Etapa, Ate Vitarte, Lima, Peru

[2] Department of Atmospheric Sciences, University of Hawai'i at Mānoa, Honolulu, HI, USA

[3] Centro de Estudios Avanzado en Zonas Áridas (CEAZA), Coquimbo, Chile

[4] Departamento de Biología, Facultad de Ciencias del Mar, Universidad Católica del Norte, Coquimbo, Chile

[5] Laboratoire d'Etudes en Géophysique et Océanographie Spatiales, Toulouse, France